ORIGINAL ARTICLE

A C G publications

Rec. Nat. Prod. 18:4 (2024) 405-418

records of natural products

Hydroxytyrosol-1-Glucopyranoside Alleviates Senescence via Nrf2 and AMPK Signaling Pathway

Yang Guo [#], Bo Zhang [#], Yongzhi Han, Muhammad Waleed Iqbal, Jia Wang, Xiaolin Shen, Hao Liang, Xinxiao Sun* and Qipeng Yuan*

State Key Laboratory of Chemical Resource Engineering, College of Life Science and Technology, Beijing University of Chemical Technology, Beijing 100029, China

(Received March 09, 2024; Revised April 30, 2024; Accepted May 03, 2024)

Abstract: Hydroxytyrosol-1-glucopyranoside (HTG) is a natural phenylethanol glycoside with promising anti-aging properties. In this study, we developed a biotransformation and purification process to effectively prepare high-purity HTG. We constructed *E. coli* strains expressing the glycosyltransferase gene UGT85A1 and UDP-glucose enhancing genes *pgm* and *galU*. By optimizing gene expression, the best strain produced 6.8 g/L HTG at 48 hours in fed-batch fermentation. Among the five different macroporous resins tested, SP825L performed the best and was employed to purify HTG from the culture broth. By optimizing the adsorption and desorption conditions, the purity and the recovery percentage reached 81.7% and of 82.4%, respectively. The purity was improved to 95.2% by further purification through preparative chromatography. The anti-aging effects of HTG were evaluated in both cells and mice. The results demonstrated its capacity to enhance cellular antioxidant capacity, reduce apoptosis, and decrease the release of senescence-associated secretory phenotype (SASP), effectively mitigating D-galactose-induced cell senescence. The potential mechanism of action suggests that HTG activates the AMPK and Nrf2 signaling pathways to protect mice from liver injury. This study suggests promising application of HTG in cosmetic and nutraceutical fields.

Keywords: Antioxidant; anti-aging; macroporous resin; hydroxytyrosol-1-glucopyranoside.

1. Introduction

Aging is a complex and evolving biological phenomenon characterized by an increasing decline in the performance of numerous tissues and organs. A crucial feature of aging is the accumulation of cellular senescence, which is triggered by different internal and external stresses [1]. Excessive senescent cell accumulation may inhibit tissue regeneration, whereas cell cycle arrest induces the establishment of a senescence-associated secretory phenotype (SASP), distinguished by different morphological, transcriptional, epigenetic, and metabolic alterations [2]. An array of age-related conditions, including diabetes, cancer, osteoporosis, neurological illnesses, cardiovascular conditions, and immunological dysfunction, have been correlated to aging [3, 4]. Medications focusing on

* Corresponding author: E-Mail: sunxx@mail.buct.edu.cn (Q. Sun); yuanqp@mail.buct.edu.cn (Q.Yuan)
# These authors have contributed equally to this work.

The article was published by ACG Publications
http://www.acgpubs.org/journal/records-of-natural-products July-August 2024 EISSN:1307-6167
DOI: http://doi.org/10.25135/rnp.460.2403.3166
Available online: July 14, 2024

biological mechanisms such as nutrition sensing and cellular senescence provide appealing techniques for slowing aging and mitigating age-related physiological deterioration. In recent years, medicines such as metformin (MET) [5, 6], rapamycin analogues [7, 8], senolytics [9], sirtuin activators [10], NAD^+ precursors [11, 12], among others, have shown anti-aging properties, while further research is required to verify their effectiveness.

Natural phenolic compounds, such as hydroxytyrosol and salidroside, possess strong anti-aging benefits. Hydroxytyrosol, mostly found in olives, is a natural bioactive molecule renowned for its varied spectrum of actions, including antioxidation, anti-aging, anti-inflammation, and anti-cancer properties [13, 14]. However, it is an oily and unstable liquid that is unsuited for long-term preservation. Salidroside, the major active component of Rhodiola rosea, has anti-aging, anti-hypoxia, anti-fatigue, anti-inflammatory, anti-radiation, and anti-cancer properties, among other benefits [15], and has found applications in healthcare and skincare products. Similarly, Hydroxytyrosol-1-glucopyranoside (HTG), a compound extracted from the plant *Sargentodoxa cuneata* (Oliv.), is a glycosylated form of hydroxytyrosol and a hydroxylated derivative of salidroside. Studies have shown that it can protect mice from dextran sulfate sodium (DSS) and sepsis induced acute pulmonary injury[16, 17], and has the potential to mitigate acute liver failure induced by acetaminophen [18].

To delve into the potential of HTG, an effective preparation procedure must be developed. Typically, HTG is obtained by plant extraction processes [16], which suffer from drawbacks such as low yield, extended cultivation periods, and complex purification processes. Microbial biosynthesis offers a sustainable and economically feasible alternative for producing natural plant compounds. In previous researches, pathways for synthesizing hydroxytyrosol [19] and salidroside [20] have been constructed, achieving effective biosynthesis. Another study reported that hydroxytyrosol was synthesized via microbial biosynthesis, followed by extraction and conversion to HTG using an *E. coli* strain expressing glycosyltransferase UGT85A1 from *Arabidopsis thaliana*, with a conversion ratio of approximately 50% [21].

Currently, limited research has been conducted on HTG's anti-aging properties. Given that glycosylation improves water solubility, stability, and bioavailability, and the addition of a phenol hydroxyl group increases antioxidant capacity, HTG may have considerable anti-aging benefits. Our study aims to establish a robust preparation method to unlock the anti-aging potential of HTG. Diverging from conventional plant extraction techniques, which come with inherent limitations, we employ whole-cell biotransformation to synthesize HTG. Subsequent purification utilizing macroporous resin and preparative chromatography yields high-purity HTG. Moreover, our study pioneers the investigation of HTG's anti-aging efficacy using a D-galactose (D-gal) treated senescence model, shedding light on its potential mechanism of action and opens up a new direction for researching HTG activity.

2. Materials and Methods

2.1. Experimental Materials

Macroporous resins were obtained from Greenherbs Science and Technology (Beijing, China). The HTG standard was purchased from ChemFaces (Wuhan, China). D-gal, NMN, and MET were purchased from Solarbio (Beijing, China). The primary and secondary antibodies were obtained from Santa Cruz (CA, USA)

2.2. Production of HTG via Bioconversion

The strains and plasmids utilized in this work are presented in Supplementary Tables 1 and 2, respectively. The plasmids pZE12-luc (high copy) and pCS27 (medium copy) were employed for gene expression. The recombination plasmids were created using the digestion and ligation procedure. E. coli strain BW25113 was transformed with the plasmids, resulting in strains HTG01, HTG02, and HTG03. After 12 h of growth in LB medium, the seed cultures were transferred to 50 mL of M9 media and shaken at 37°C. IPTG (0.5 mM) was introduced after 3 h to stimulate gene expression. For the

fed-batch experiment, 100 mL of seed culture was moved to a 3 L bioreactor containing 900 mL of M9 media.

2.3. HPLC Analysis

HTG was analyzed and quantified using the modified reverse phase HPLC method [20] .

2.4. Purification of HTG by Macroporous Resin Absorption and Preparative Chromatography

HTG was purified using five macroporous resins of varying polarity (AB-8, HPD-300, HPD-600, SP207, and SP825L) (Supplementary Table 3). After adding an adequate proportion of supernatant of fermentation broth to the resins, HTG adsorption was carried out at 25°C and 100 rpm for 12 h. The resins were cleaned with deionized water, and HTG was extracted with a 30% ethanol aqueous solution (*v*:*v*). The static adsorption kinetics curve was constructed, and the desorption rate of HTG at various ethanol concentrations was observed. Dynamic adsorption and desorption experiments were carried out by column chromatography. Next, the purity and recovery rate of the freeze-dried items were determined. HTG was further purified by preparative chromatography with a C18 column and a mobile phase of 30% methanol aqueous solution (*v*:*v*). HTG components were collected and freeze-dried.

2.5. Cell Culture and Treatments

Human foreskin fibroblasts (HFF) were procured from Hunan Fenghui Biotechnology Co., Ltd. A suspension of HFF single cells was added to 96-well microplates. The cells were then treated with D-gal for 24 h to promote cell aging. The cells were further experimented with HTG or MET to see which had a more significant anti-aging effect.

2.6. Senescence-associated β-galactosidase (SA-β-Gal) Staining

SA-β-Gal serves as a widely embraced marker to detect cellular aging [22]. HFF cells were pre-treated with HTG or MET for 24 h before being exposed to D-gal for another 24 h. After the test, the assay was done using an SA-β-Gal staining kit (Beyotime).

2.7. Real-time Fluorescence Quantitative PCR and Western Blot

RNA extraction and cDNA synthesis were carried out for PCR amplification. The primers used in the experiment are listed in Supplementary Table 4. Western blot analysis was used to measure the target protein in liver tissue.

2.8. Detection of Reactive Oxygen Species (ROS)

Intracellular total ROS levels were measured utilizing a fluorescence probe [23]. Cells were treated with DCFH-DA solution (Beyotime), incubated at 37°C for 20 min, and examined using fluorescence microscopy.

2.9. Detection of Biochemical Indices

The cellular activities of superoxide dismutase (SOD) and the levels of glutathione (GSH) were evaluated. Additionally, the activities of both SOD and catalase (CAT), as well as the levels of malondialdehyde (MDA) in liver tissue, were examined in accordance with the protocols provided by the respective assay kits (Nanjing Jiancheng).

2.10. Investigation of Nuclear Structure in Senescent Cells

Nuclear morphology was scrutinized using DAPI, a dye that fluoresces upon binding to DNA with high specificity [24]. The steps were performed following the instructions in the DAPI staining kit (Beyotime).

2.11. Measurement of Apoptotic Cells

Analysis of cell apoptosis in different phases by flow cytometry [25], followed by the detection of related apoptotic proteins. The Annexin V-FITC/Pl staining kit from Beyotime was used to detect apoptotic HFF cells and determine the rate of apoptosis. The Caspase 3/9 activity test kit (Beyotime) was utilized to detect apoptosis in HFF cells.

2.12. Grouping and Administration of Mice

Male C57BL/6J mice aged 6 weeks were procured from Beijing Vital River Laboratory Animal Technology Co., Ltd. After a one-week acclimatization period, the mice were randomly allocated to one of five groups, each containing seven mice: control, D-gal, D-gal + HTG (20 mg/kg b.w., low dosage; 40 mg/kg b.w., high dose), and D-gal + NMN (100 mg/kg b.w., positive control). The control group got normal saline. D-gal therapy included subcutaneous injections at 400 mg/kg b.w. for weeks 1-4 and 800 mg/kg b.w. for weeks 5-8. In the subsequent three groups, HTG and MET were given orally two hours after the D-gal injection. After 8 weeks, the mice were killed and new liver tissue was harvested.

2.13. Hematoxylin-Eosin (H&E) Staining

H&E staining is employed for histo-morphological observations. This method reveals subtle structural changes within and around the cell nucleus through specific chemical treatments and staining [26]. The liver tissue was preserved in 4% paraformaldehyde, then embedded in paraffin wax, sliced to a thickness of 4 micrometers, subjected to staining, and examined under an optical microscope.

2.14. Detection the Expression Levels of Inflammatory Cytokines in the Liver.

Levels of tumor necrosis factor-alpha (TNF-α), interferon-gamma (IFN-γ), and interleukin-6 (IL-6) in liver tissues were quantified using ELISA kits (Mlbio).

2.15. Statistical Analysis

Data analysis was performed using GraphPad Prism software. Results were presented as Mean ± S.D., with statistical significance defined as $p < 0.05$. $^{\#}p < 0.05$, $^{\#\#}p < 0.01$, $^{\#\#\#}p < 0.001$, *vs*. control group, * $p < 0.05$, ** $p < 0.01$, *** $p < 0.001$ *vs*. D-gal-treated group.

3. Results and Discussion

3.1. Production of HTG from Hydroxytyrosol via Biotransformation

To obtain sufficient quantity of HTG for the activity analysis, we initially established a convenient and efficient biotransformation process using hydroxytyrosol as the precursor. Hydroxytyrosol can be enzymatically converted to HTG by glucosyltransferase UGT85A1 sourced from *Arabidopsis thaliana* [21] (Figure 1A). Co-expression of gene UGT85A1 with the UDPG-enhancing-module (comprising genes *pgm* and *galU*) was implemented. To optimize their expression

levels, three strains (HTG01, HTG02, and HTG03) were constructed. Results indicated that strain HTG01, harbouring plasmids pZE-UGT85A1 and pCS-pgm-galU, exhibited the highest performance. When supplied with 1 g/L hydroxytyrosol, HTG01 yielded 1.8 g/L HTG within 48 h. Furthermore, the biotransformation process was scaled up in a 3 L bioreactor. Upon feeding with 4 g/L hydroxytyrosol, strain HTG01 produced 6.8 g/L HTG within the same timeframe (Figure 1C). Following bioreactor cultivation, the culture broth was centrifugated, and the supernatant was utilized for subsequent purification steps.

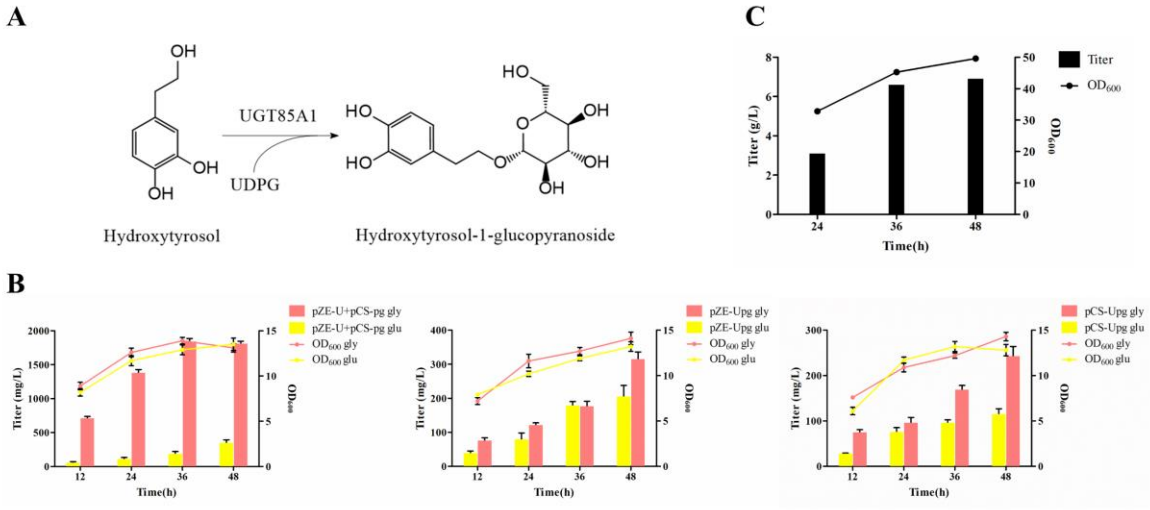

Figure 1. (**A**) Biotransformation pathway of HTG. (**B**) Different strains were used to produce HTG. (**C**) Fed-batch fermentation to produce HTG.

3.2. Isolation and Purification of HTG

We evaluated the performance of five different macroporous resins, among which SP825L exhibited the highest adsorption capacity (34.4 mg/g) and the most efficient desorption rate (87.2%). Consequently, SP825L was chosen to purify HTG (Figure 2A). The adsorption equilibrium time of SP825L resin was determined to be 150 min (Figure 2B). Desorption efficiency was significantly influenced by the concentration of ethanol, with 30% ethanol identified as the optimal desorption concentration for HTG (Figure 2C). HTG shares a similar polarity with 30% ethanol based on the principle of similarity compatibility. The leakage point was observed when the mass concentration of the effluent reached 1/10 of the sample liquid, indicating a maximum loading volume of 3 BV (Figure 2D). Experimental data revealed that when the elution volume reached 1.5 BV, the HTG content in the eluent was notably low (Figure 2E), suggesting that this point had eluted the majority of HTG adsorbed by the macroporous resin. Therefore, an elution volume of 1.5 BV was selected. After lyophilization, the purity of HTG reached 81.7%, with a recovery rate of 82.4%. After preparative chromatography purification, the purity was further increased to 95.2%, which is sufficient for the subsequent activity analysis (Figure 2F).

Hydroxytyrosol-1-glucopyranoside

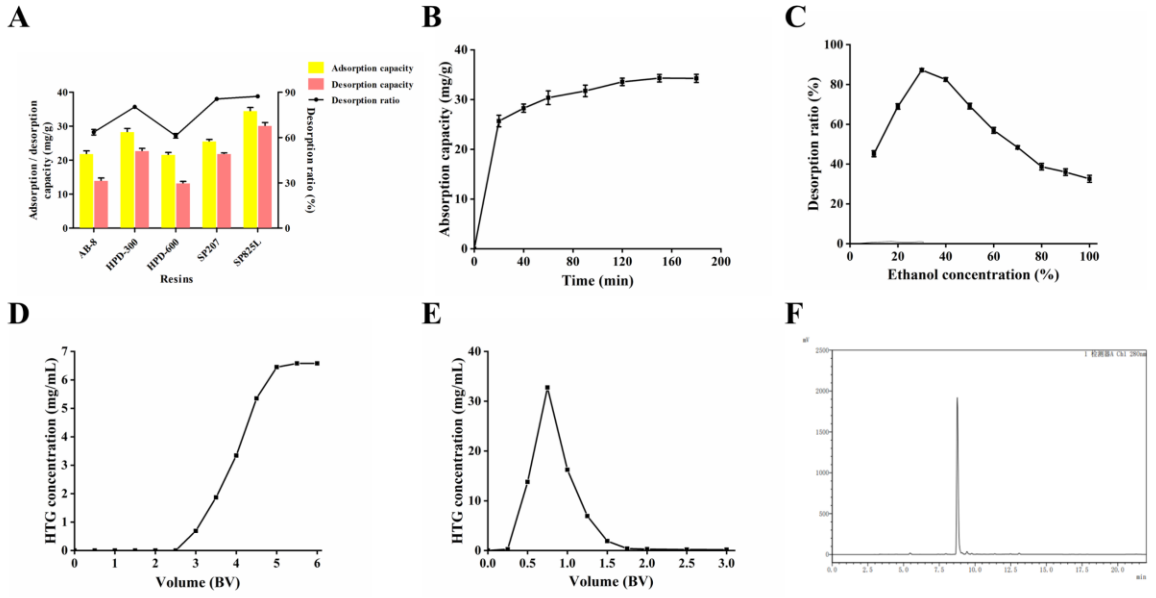

Figure 2. (**A**) Adsorption and desorption capacity, and desorption ratio of HTG on different resins. (**B**) The curve depicting the kinetics of adsorption on the SP825L resin. (**C**) Ethanol concentration effect on desorption ratio. (**D**) Leakage curve on SP825L resin. (**E**) Dynamic desorption curve on SP825L resin. (F) Preparative chromatography purification.

3.3. HTG Promotes Cell Viability in D-gal-induced Senescent Model

The D-gal-based aging model is widely employed due to its simplicity, cost-effectiveness, and consistent outcomes [27], with HFF cells frequently utilized to simulate aging. Hence, different concentrations of D-gal were applied to HFF cells to establish the aging model. According to previous reports, an appropriate inhibition rate on cell viability falls within the 30-50% range. Accordingly, a concentration of 60 g/L D-gal was selected for subsequent experiments (Figure 3A). To assess the anti-aging potential, the promising anti-aging drug metformin was employed as a positive control. The impacts of HTG and MET on cell growth were examined, revealing a dose-dependent growth-promoting effect of HTG and MET up to concentrations of 150 μM and 2 mM, respectively (Figure 3B). Consequently, for subsequent experiments, the working concentrations of HTG were set at 50, 100, and 150 μM, while MET was maintained at 2 mM as the control.

Cells were initially exposed to varying concentrations of HTG for 24 h, followed by a 24 h treatment with 60 g/L D-gal to confirm HTG's protective effect against D-gal-induced senescence. Results showed a significant decrease in cell viability in the D-gal treatment group compared to the control. However, pre-treatment with HTG dose-dependently mitigated D-gal-induced cell death. The protective effect of 150 μM HTG was comparable to that of 2 mM MET (Figure 3C). SA-β-Gal activity, indicative of cell senescence, was evaluated. HTG pretreatment significantly reduced the number of SA-β-Gal positive cells, with similar results observed in the MET group (Figure 3D). mRNA levels of the cell cycle regulatory proteins P53 and P21, significantly upregulated during cell aging [28], were reduced by HTG compared to the D-gal group (Figure 3E). These findings suggest that HTG and MET can mitigate D-gal-induced damage in HFF cells, with HTG exhibiting similar effects to MET at lower concentrations.

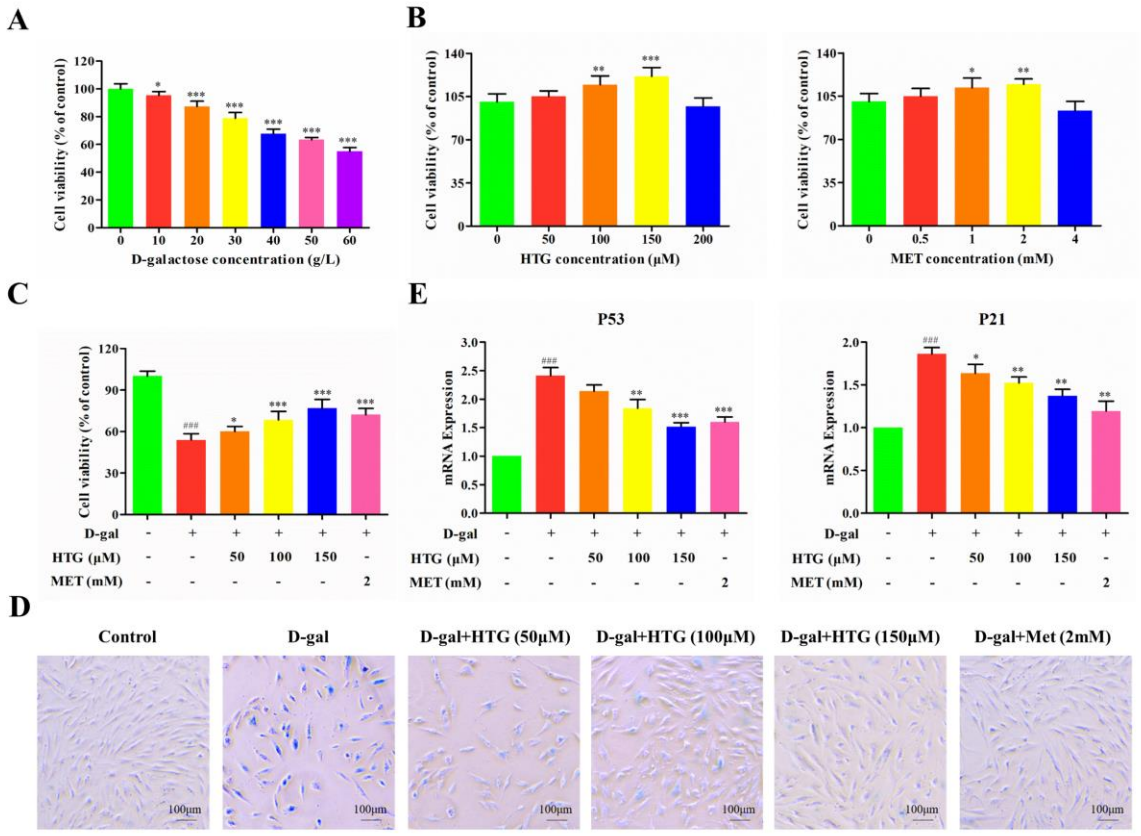

Figure 3. (**A**) Effect of D-gal on proliferation of HFF cells. (**B**) Effect of HTG and MET on HFF cells viability. (**C**) Impact of HTG on the viability of HFF cells subjected to D-gal-induced aging. (**D**) SA-β-Gal staining images. (**E**) mRNA levels of p53 and p21 were examined in cells from each group.

3.4. HTG Inhibits ROS Production and Enhances Antioxidant Capacity

D-gal can accelerate intracellular ROS production, leading to oxidative stress [29]. Thus, the effect of HTG on the antioxidative ability of D-gal-treated cells was studied. Intracellular ROS levels were assessed using the DCFH-DA method. The fluorescence intensity of D-gal was higher than that of the control group. Following HTG pretreatment, the fluorescence intensity exhibited a dose-dependent decrease. Similar reductions in fluorescence intensity were observed in the MET group (Figure 4A). In addition, D-gal treatment significantly decreased GSH and SOD activity. However, these declines in GSH levels and enzyme activity were gradually attenuated with increasing doses of HTG (Figure 4B). These results indicate that HTG alleviates oxidative stress caused by D-gal, and bolsters the antioxidant defenses in aging cells.

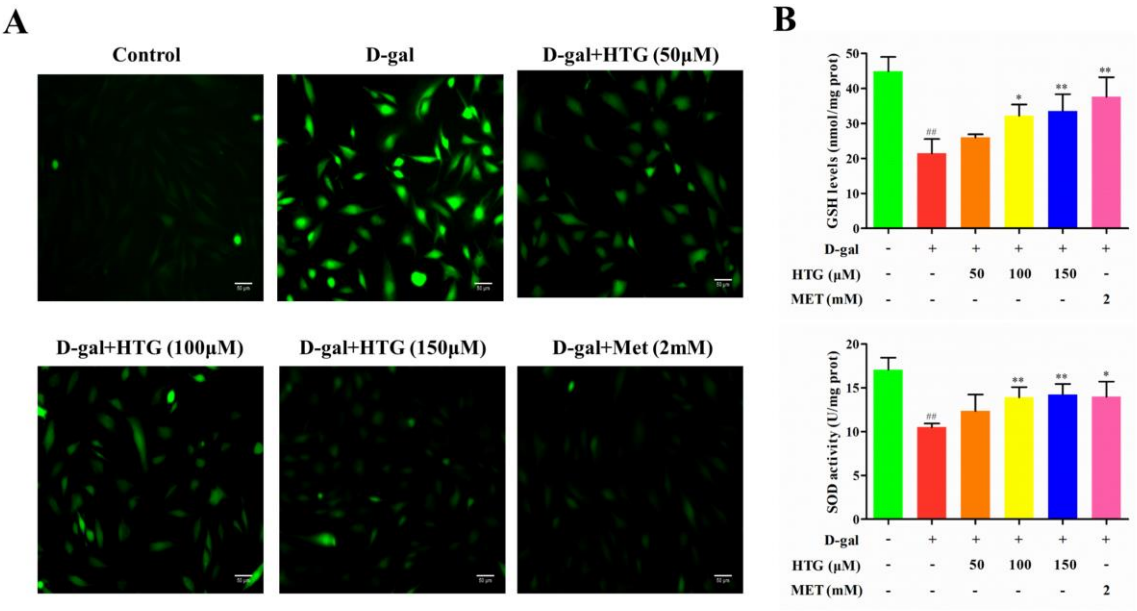

Figure 4. (**A**) Effect of HTG on ROS in HFF cells. (**B**) Effects of HTG on the levels of GSH and the activity of SOD in HFF cells.

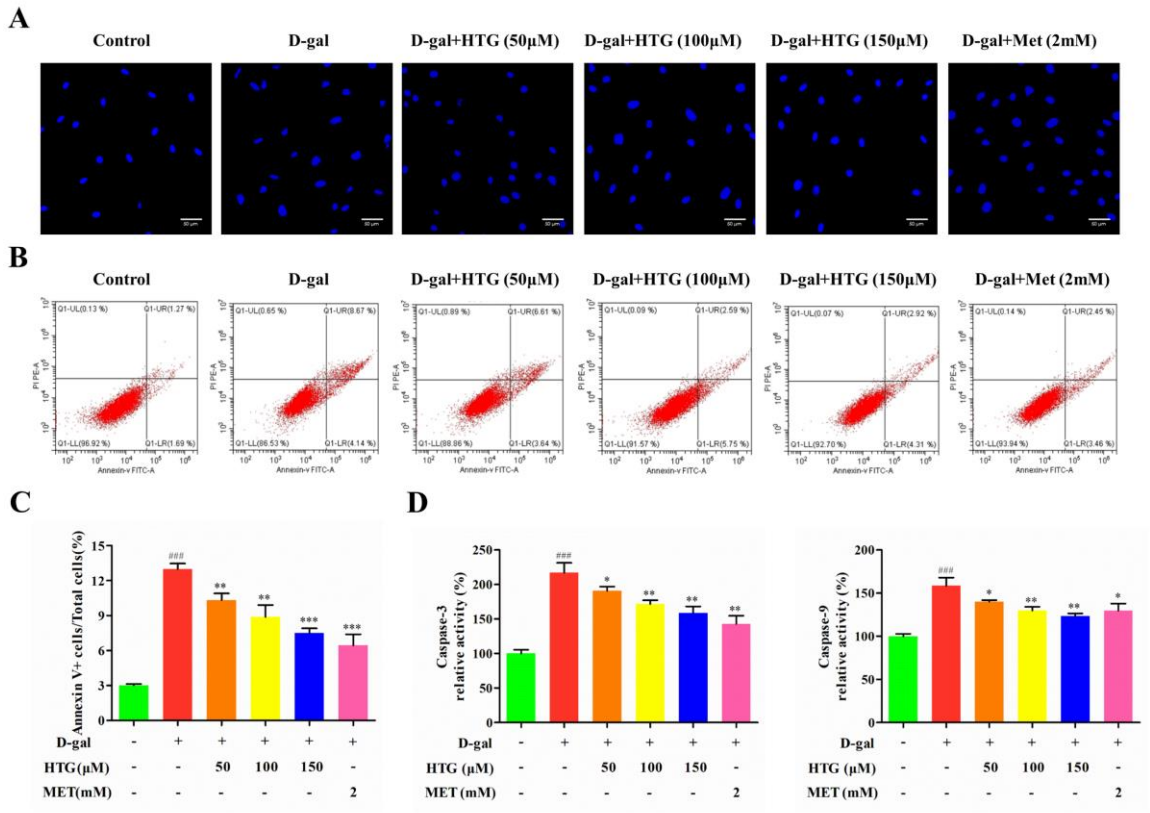

Figure 5. (**A**) DAPI staining. (**B-C**) Apoptosis rates were detected with flow cytometry. (**D**) Caspase-3/9 protein expression.

3.5. HTG Attenuates Apoptosis

The excess of ROS in mitochondria may result in mitochondrial injury, which leads to the release of proapoptotic material from mitochondria and ultimately induces apoptosis [30]. Next, we further observed the effect of HTG on D-gal induced apoptosis of HFF cells by observing the morphology of the nucleus under a fluorescence microscope. The D-gal model group exhibited apoptotic features such as chromatin condensation and peripheral aggregation. Pretreatment with HTG and MET reduced these phenomena (Figure 5A). Figure 5B and C showed that D-gal treatment caused apoptosis of cells, and the proportion of apoptotic cells was significantly higher than that in the normal group. After HTG and MET pretreatment, the percentage of apoptosis of senescent cells was decreased. Additionally, apoptosis-associated proteins, Caspase-3 and Caspase-9, were assessed. The results indicated that the D-galactose treatment led to a significant increase in their expression levels, compared to the normal group. However, the expression of apoptosis protein was significantly decreased after HTG and MET pretreatment. (Figure 5D). The apoptotic rate and expression of apoptotic protein in senescent cells were detected, suggesting that HTG could alleviate D-gal induced apoptosis.

3.6. HTG Reduces SASP Release

Senescent cells produce proinflammatory cytokines and proteases, collectively called SASP [2]. To further explore the protective effects of HTG against oxidative stress induced by D-gal, we evaluated the levels of cellular inflammatory cytokines. Our findings indicated that there was an expression of various inflammatory markers. However, HTG and MET pretreatments significantly reduced these levels (Figure 6).

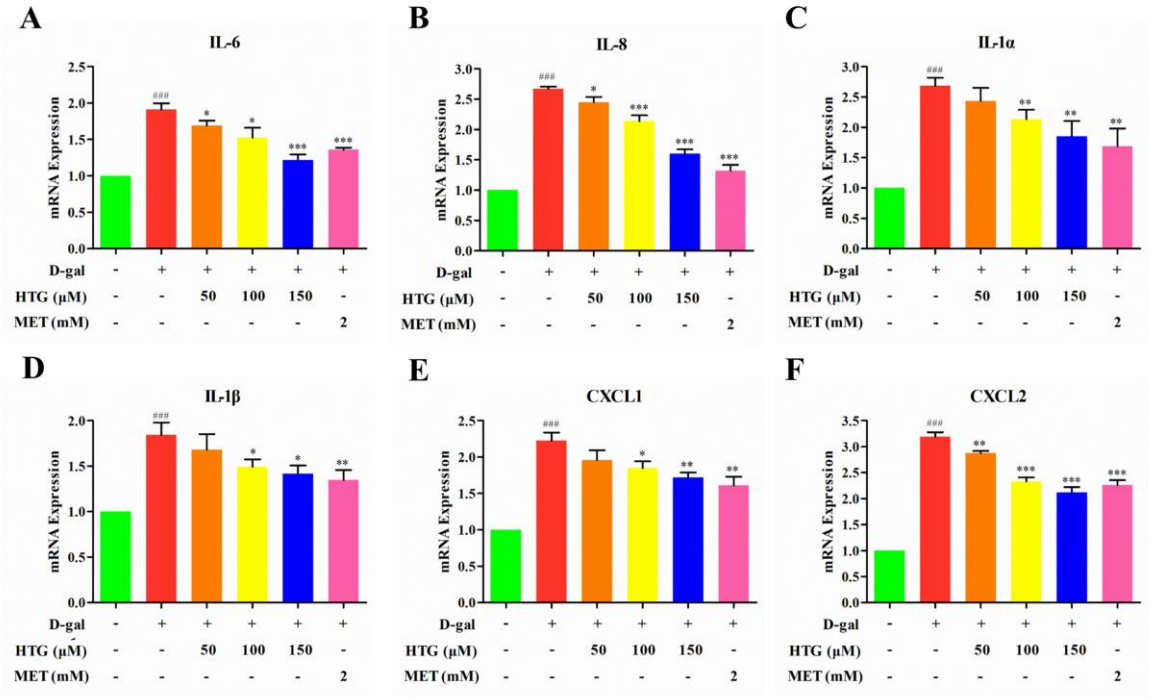

Figure 6. mRNA levels of SASP in HFF cells detected by qRT-PCR.

3.7. Effect of HTG on Body Weight and Liver Index in D-gal-induced Mice

Aging typically reduces organ quality and affects various organ indicators [31]. NMN has effectively mitigated age-related physiological decline in mice [11], thus serving as a positive control. We administered HTG and NMN daily for 8 weeks to evaluate the protective effect of HTG and NMN on D-gal-induced liver tissue injury in mice. Compared to the control group, the D-gal group displayed a significant decrease in liver index. In contrast, both the HTG and NMN treatment groups experienced a progressive rise in liver index in comparison to the D-gal group. Moreover, initial and final body weights of each mouse group were documented (Table 1). Mice treated with D-gal experienced less weight gain than the control group, whereas HTG-treated mice demonstrated dose-dependent weight gain. NMN-treated mice gained more weight than those treated with HTG. The findings suggest that HTG could offer a protective effect against liver injury induced by D-gal.

Table 1. Changes of body weight and liver index

Groups	Liver Index (mg/g)	Initial Body Weight (g)	Final Body Weight (g)
Control	50.09 ± 1.19	22.50 ± 0.67	27.65 ± 1.01
D-gal	42.27 ± 2.87$^{###}$	22.01 ± 0.53	25.66 ± 1.29$^{#}$
D-gal + HTG (20 mg/kg b.w.)	45.03 ± 2.83	22.13 ± 0.47	25.93 ± 1.00
D-gal + HTG (40 mg/kg b.w.)	46.84 ± 2.81*	22.62 ± 0.87	26.75 ± 0.81
D-gal + NMN (100 mg/kg b.w.)	48.05 ± 2.31**	21.96 ± 0.93	26.24 ± 1.24

3.8. Effect of HTG on Hepatic Damage in Mice Induced by D-gal.

To further assess the protective effects of HTG on hepatic tissue, we conducted H&E staining on liver sections (Figure 7A). Results revealed disordered liver tissue structure, hepatocyte atrophy, increased fat vacuoles, and localized infiltration of inflammatory cells in the D-gal group. However, with the intervention of HTG and NMN, these changes gradually disappeared. The accumulation of D-gal in the body can produce excessive ROS, inducing oxidative stress. Measurement of MDA levels can directly reflect plasma membrane peroxidation [32]. Antioxidant systems encompass endogenous molecules such as SOD, CAT, and non-enzymatic antioxidants [33]. In our study, we found that MDA was significantly increased by D-gal treatment and SOD and CAT levels were decreased (Figure 7B). However, the administration of both HTG and NMN has successfully counteracted this impact, suggesting that HTG is capable of mitigating oxidative stress through the reduction of lipid peroxidation and the enhancement of antioxidant enzyme activities. Next, we assessed the inflammatory factor levels in liver tissues. Compared to the control group, D-gal treatment significantly elevated inflammatory factor levels, which HTG treatment effectively alleviated in D-gal-treated mouse livers (Figure 7C).

AMPK is pivotal in regulating metabolism and maintaining energy homeostasis [34], while Nrf2 is a crucial transcription factor inducing the body's antioxidant response [35]. To elucidate HTG's protective mechanism, we analyzed protein expression via western blotting. In comparison to the control group, the levels of AMPK and SIRT1 in D-gal group were significantly decreased, while HTG and NMN were gradually increased after treatment (Figure 7D). While the levels of Nrf2 and HO-1 proteins were observed to be significantly diminished in the D-gal group, these levels were notably elevated in the groups treated with HTG and NMN (Figure 7E). Our results indicate that HTG may increase the levels of AMPK and Nrf2 signaling pathways to protect the liver against oxidative damage.

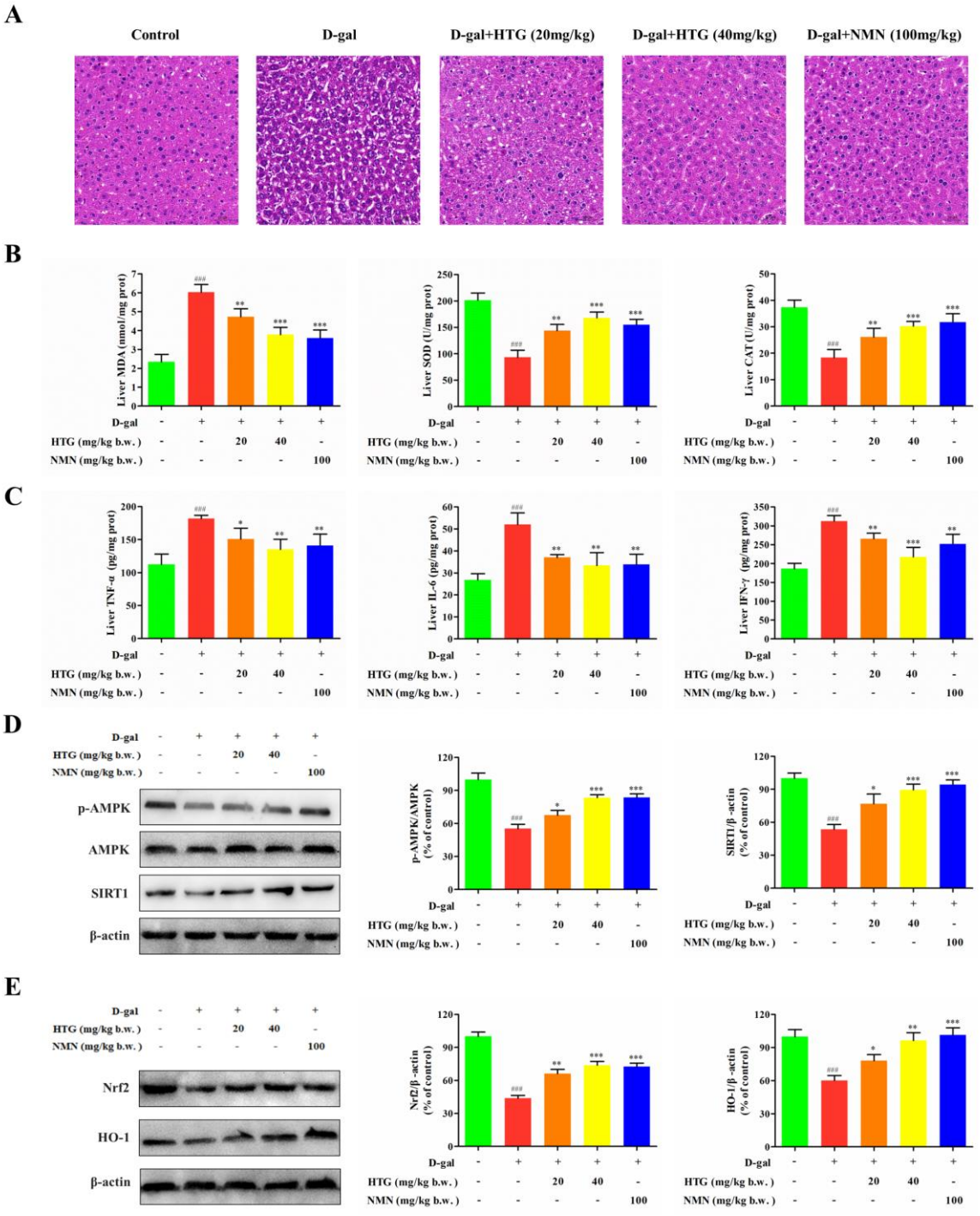

Figure 7. (**A**) H&E staining of liver. (**B**) Effects of HTG on the contents of MDA, SOD and CAT in mice liver. (**C**) Effect of HTG on inflammatory cytokines in mice liver. (**D**-**E**) Effect of HTG on the expression of AMPK and Nrf2 pathway protein in liver.

4. Conclusion

This study successfully developed a biotransformation and purification method for HTG and evaluated its anti-aging effects *in vitro* and *in vivo*. The findings indicate that HTG boosts the cells' ability to combat oxidative stress, diminishes the occurrence of apoptosis, and lessens the secretion of the SASP, thereby significantly mitigating cell senescence triggered by D-gal. Additionally, our findings suggest that HTG mitigates D-gal-induced liver injury in mice by upregulating the expression of AMPK and Nrf2 proteins. These findings lay a foundation for applying HTG in healthcare products, cosmetics, and other fields, offering a promising approach to anti-aging.

Abbreviations

HTG, Hydroxytyrosol-1-glucopyranoside; SASP, Senescence-associated secretory phenotype; D-gal, D-galactose; AMPK, AMP-activated protein kinase; Nrf2, Nuclear factor erythroid 2-related factor 2; MET, Metformin; NMN, Nicotinamide Mononucleotide; IPTG, Isopropyl β-D-1-thiogalactopyranoside; HPLC, High-performance liquid chromatography; HFF, Human foreskin fibroblasts; SA-β-Gal, Senescence-associated β-galactosidase; ROS, Reactive oxygen species ; SOD, Superoxide dismutase; CAT, Catalase; GSH, Glutathione; MDA, Malondialdehyde; DAPI, 4',6-diamidino-2-phenylindole; TNF-α, Tumor necrosis factor-alpha; IFN-γ, Interferon-gamma; IL-6, Interleukin-6; IL-8, Interleukin-8; IL-1α, Interleukin-1α; IL-1β, Interleukin-1β; CXCL1, C-X-C motif chemokine ligand 1; CXCL2, C-X-C motif chemokine ligand 2; b.w., body weight; H&E, Hematoxylin-eosin ; ELISA, Enzyme-linked immunosorbent assay; BV, Bed volume; SIRT1, Sirtuin-1; HO-1, Heme oxygenase-1.

Acknowledgments

This work was supported by National Key Research and Development Program of China (2021YFC2101500), Key Research and Development Program of Guangdong Province (2022B1111080003), National Natural Science Foundation of China (22238001, 22322802, 22078011).

Declarations

Ethics Approval

We ensured that all animal manipulations comply with the relevant laws and guidelines of the Animal Ethics Committee. The study was conducted in accordance with the Declaration of Helsinki. All mouse experiments were conducted at Beijing Viewsolid Biotechnology Co., Ltd. and approved by the Institutional Animal Committee of Beijing Viewsolid Biotechnology Co., Ltd. (SCXK 2021−0010). To prevent the effects of euthanasia injection drugs on organ indexes in mice, all mice were euthanized by cervical dislocation in this study.

Competing Interests

The authors declare no competing interests.

ORCID
Yang Guo: 0009-0001-9420-5909
Bo Zhang: 0009-0003-8088-8811
Yongzhi Han:0009-0002-4612-5338
Mohammad Wael Iqbal: 0009-0001-8479-2054
Jia Wang: 0000-0002-7218-2224
Xiaolin Shen: 0000-0002-6969-2952

Hao Liang: 0000-0002-4799-882X
Xinxiao Sun: 0000-0001-5590-6473
Qipeng Yuan: 0000-0002-7899-1487

References

[1] Z. Li, Z. Zhang, Y. Ren, Y. Wang, J. Fang, H. Yue, S. Ma and F. Guan (2021). Aging and age-related diseases: from mechanisms to therapeutic strategies, *Biogerontology* **22**, 165-187.

[2] N. Ohtani (2022). The roles and mechanisms of senescence-associated secretory phenotype (SASP): can it be controlled by senolysis? *Inflamm. Regen*. **42**, 11.

[3] L. Partridge, J. Deelen and P. E. Slagboom (2018). Facing up to the global challenges of ageing, *Nature* **561**, 45-56.

[4] M. Kritsilis, V. R. S, P. N. Koutsoudaki, K. Evangelou, V. G. Gorgoulis and D. Papadopoulos (2018). Ageing, cellular senescence and neurodegenerative disease, *Int. J. Mol. Sci*. **19**, 2937.

[5] A. Martin-Montalvo, E. M. Mercken, S. J. Mitchell, H. H. Palacios, P. L. Mote, M. Scheibye-Knudsen, A. P. Gomes, T. M. Ward, R. K. Minor, M. J. Blouin, M. Schwab, M. Pollak, Y. Zhang, Y. Yu, K. G. Becker, V. A. Bohr, D. K. Ingram, D. A. Sinclair, N. S. Wolf, S. R. Spindler, M. Bernier and R. De Cabo (2013). Metformin improves healthspan and lifespan in mice, *Nat. Commun*. **4**, 2192. 10.1038/ncomms3192

[6] F. Cabreiro, C. Au, K. Y. Leung, N. Vergara-Irigaray, H. M. Cocheme, T. Noori, D. Weinkove, E. Schuster, N. D. Greene and D. Gems (2013). Metformin retards aging in C. elegans by altering microbial folate and methionine metabolism, *Cell* **153**, 228-239.

[7] D. W. Lamming, L. Ye, D. M. Sabatini and J. A. Baur (2013). Rapalogs and mTOR inhibitors as anti-aging therapeutics, *J. Clin. Invest*. **123**, 980-989.

[8] D. E. Harrison, R. Strong, Z. D. Sharp, J. F. Nelson, C. M. Astle, K. Flurkey, N. L. Nadon, J. E. Wilkinson, K. Frenkel, C. S. Carter, M. Pahor, M. A. Javors, E. Fernandez and R. A. Miller (2009). Rapamycin fed late in life extends lifespan in genetically heterogeneous mice, *Nature* **460**, 392-395.

[9] L. Zhang, L. E. Pitcher, V. Prahalad, L. J. Niedernhofer and P. D. Robbins (2021). Recent advances in the discovery of senolytics, *Mech. Ageing Dev*. **200**, 111587.

[10] A. E. Kane and D. A. Sinclair (2018). Sirtuins and NAD^+ in the development and treatment of metabolic and cardiovascular diseases, *Circ. Res*. **123**, 868-885.

[11] K. F. Mills, S. Yoshida, L. R. Stein, A. Grozio, S. Kubota, Y. Sasaki, P. Redpath, M. E. Migaud, R. S. Apte, K. Uchida, J. Yoshino and S. I. Imai (2016). Long-term administration of nicotinamide mononucleotide mitigates age-associated physiological decline in mice *Cell Metab*. **24**, 795-806.

[12] J. Yoshino, K. F. Mills, M. J. Yoon and S. I. Imai (2011). Nicotinamide mononucleotide, a key NAD^+ intermediate, treats the pathophysiology of diet-and age-induced diabetes in mice, *Cell Metab*. **14**, 528-536.

[13] R. W. Owen, A. Giacosa, W. E. Hull, R. Haubner, G. Wurtele, B. Spiegelhalder and H. Bartsch (2000). Olive-oil consumption and health: the possible role of antioxidants, *Lancet Oncol*. **1**, 107-112.

[14] R. M. De Pablos, A. M. Espinosa Oliva, R. Hornedo Ortega, M. Cano and S. Arguelles (2019). Hydroxytyrosol protects from aging process via AMPK and autophagy; a review of its effects on cancer, metabolic syndrome, osteoporosis, immune-mediated and neurodegenerative diseases, *Pharmacol. Res*. **143**, 58-72.

[15] X. Zhang, L. Xie, J. Long, Q. Xie, Y. Zheng, K. Liu and X. Li (2021). Salidroside: A review of its recent advances in synthetic pathways and pharmacological properties, *Chem. Biol. Interact*. **339**, 109268.

[16] D. Li, Y. Zhuo, Q. Zhang, L. Zhang, S. Zhang, Y. Lv, C. Li, L. Cui, X. Guan, L. Yang and X. Wang (2019). Purification of 3, 4-dihydroxyphenylethyl alcohol glycoside from *Sargentodoxa cuneata* (Oliv.) Rehd. et Wils. and its protective effects against DSS-induced colitis, *Sci. Rep*. **9,** 3222.

[17] Y. Zhuo, D. Li, L. Cui, C. Li, S. Zhang, Q. Zhang, L. Zhang, X. Wang and L. Yang (2019). Treatment with 3,4-dihydroxyphenylethyl alcohol glycoside ameliorates sepsis-induced ALI in mice by reducing inflammation and regulating M1 polarization, *Biomed. Pharmacother.* **116**, 109012.

[18] T. Liu, L. Yang, H. Gao, Y. Zhuo, Z. Tu, Y. Wang, J. Xun, Q. Zhang, L. Zhang and X. Wang (2022). 3,4-dihydroxyphenylethyl alcohol glycoside reduces acetaminophen-induced acute liver failure in mice by inhibiting hepatocyte ferroptosis and pyroptosis, *PeerJ*. **10**, e13082.

[19] X. Li, Z. Chen, Y. Wu, Y. Yan, X. Sun and Q. Yuan (2018). Establishing an artificial pathway for efficient biosynthesis of hydroxytyrosol, *ACS Synth. Biol*. **7**, 647-654.

[20] X. Li, Z. Zhou, W. Li, Y. Yan, X. Shen, J. Wang, X. Sun and Q. Yuan (2022). Design of stable and self-regulated microbial consortia for chemical synthesis, *Nat. Commun*. **13**, 1554.
[21] H. J. Choo, E. J. Kim, S. Y. Kim, Y. Lee, B.-G. Kim and J.-H. Ahn (2018). Microbial synthesis of hydroxytyrosol and hydroxysalidroside, *Appl. Biol. Chem*. **61**, 295-301.
[22] A. Krzystyniak, A. Gluchowska, G. Mosieniak and E. Sikora (2023). Fiji-based tool for rapid and unbiased analysis of SA-β-Gal activity in cultured cells, *Biomolecules* **13**, 362.
[23] E. Eruslanov and S. Kusmartsev (2010). Identification of ROS using oxidized DCFDA and flow-cytometry, *Methods Mol. Biol.* **594**, 57-72.
[24] B. Chazotte (2011). Labeling nuclear DNA using DAPI. *Cold Spring Harb. Protoc*. **2011**, 80-82.
[25] L. C. Crowley, B. J. Marfell, A. P. Scott and N. J. Waterhouse (2016). Quantitation of apoptosis and necrosis by Annexin V binding, propidium iodide uptake, and flow cytometry, *Cold Spring Harb. Protoc*. **2016**, 953-957.
[26] R. D. Cardiff, C. H. Miller and R. J. Munn (2014). Manual hematoxylin and eosin staining of mouse tissue sections, *Cold Spring Harb. Protoc*. **2014**, 655-658.
[27] K. F. Azman and R. Zakaria (2019). D-galactose-induced accelerated aging model: an overview, *Biogerontology* **20**, 763-782.
[28] R. Munk, A. C. Panda, I. Grammatikakis, M. Gorospe and K. Abdelmohsen (2017). Senescence-associated microRNAs, *Int. Rev. Cell Mol. Biol*. **334**, 177-205.
[29] R. Liu, J. Meng and D. Lou (2021). Adiponectin inhibits D-gal-induced cardiomyocyte senescence via AdipoR1/APPL1, *Mol. Med. Rep*. **24,** 719.
[30] H. Bayir and V. E. Kagan (2008). Bench-to-bedside review: mitochondrial injury, oxidative stress and apoptosis – there is nothing more practical than a good theory, *Crit. Care*. **12**, 206.
[31] F. Li, G. Huang, F. Tan, R. Yi, X. Zhou, J. Mu and X. Zhao (2019). *Lactobacillus plantarum* KSFY06 on d-galactose-induced oxidation and aging in Kunming mice, *Food Sci. Nutr*. **8**, 379-389.
[32] D. Tsikas (2017). Assessment of lipid peroxidation by measuring malondialdehyde (MDA) and relatives in biological samples: Analytical and biological challenges, *Anal. Biochem*. **524**, 13-30.
[33] L. He, T. He, S. Farrar, L. Ji, T. Liu and X. Ma (2017). Antioxidants maintain cellular redox homeostasis by elimination of reactive oxygen species, *Cell. Physiol. Biochem*. **44**, 532-553.
[34] A. Salminen and K. Kaarniranta (2012). AMP-activated protein kinase (AMPK) controls the aging process via an integrated signaling network, *Ageing Res. Rev*. **11**, 230-241.
[35] F. He, X. Ru and T. Wen (2020). NRF2, a ttranscription factor for stress response and beyond, *Int. J. Mol. Sci*. **21**, 4777.